



## Magneto-optical Kerr effect spectroscopy study of $2H$ -MoS<sub>2</sub>: Evidence for an interlayer $B$ -like exciton

Dibyasanakar Das <sup>1</sup>, Dipankar Jana <sup>1</sup>, Thorsten Deilmann <sup>2,\*</sup> and Sandip Ghosh <sup>1,†</sup>

<sup>1</sup>*Department of Condensed Matter Physics and Materials Science, Tata Institute of Fundamental Research, Mumbai 400005, India*

<sup>2</sup>*Institut für Festkörperteorie, Universität Münster, 48149 Münster, Germany*

 (Received 3 July 2024; revised 19 August 2024; accepted 26 August 2024; published 4 September 2024)

Magneto-optical Kerr effect spectroscopy has been used to measure the Landé  $g$ -factor of excitons in bulk  $2H$ -MoS<sub>2</sub>. For the ground state  $A_{1s}$  exciton, the adjacent interlayer  $IL_A$  exciton and the ground state  $B_{1s}$  exciton we get  $g_{A_{1s}} = -3.1 \pm 0.2$ ,  $g_{IL_A} = 10.9 \pm 0.8$  and  $g_{B_{1s}} = -3.0 \pm 0.4$ , similar to previous reports based on other measurement techniques. However on the higher energy side of  $B_{1s}$  we find another transition which we label  $IL_B$ , with  $g_{IL_B} = 10.6 \pm 1.5$ . Its presence is independently verified through the observation of a strong feature at that energy in a laser modulated photoreflectance spectrum. Based on the sign and large magnitude of  $g_{IL_B}$  and using an approximate model to explain it, we identify this as another interlayer type exciton which predominantly involves the second valence band at the  $K$  points of the Brillouin zone. The possible existence of an  $IL_B$  like exciton state is also indicated by our calculations based on density functional theory including electron-hole Coulomb interaction via the  $GW$  + Bethe-Salpeter equation.

DOI: [10.1103/PhysRevB.110.115201](https://doi.org/10.1103/PhysRevB.110.115201)

### I. INTRODUCTION

Transition metal dichalcogenide (TMDC) semiconductors of the form  $MX_2$  ( $M$ =Mo, W, Re and  $X$ =S, Se, Te) have relatively large carrier effective masses which results in exciton binding energies ( $E_b$ ) that easily exceeds thermal energy  $k_B T \sim 26$  meV at room temperature [1]. As a result several excitons and their excited state transitions are seen in TMDCs even at room temperature with consequences for device applications. This is especially true for their monolayer/few layer film forms where  $E_b$  is further enhanced due to their effective two-dimensional nature. Some of these excitons have unusual properties, such as the fairly recently identified interlayer exciton. The interlayer exciton in a bulk TMDC semiconductor, which has no equivalent in a three-dimensional hydrogenic exciton model, was first identified in  $2H$ -MoTe<sub>2</sub> [2] and later in  $2H$ -MoS<sub>2</sub> [3]. In the interlayer exciton state in  $2H$ -MoS<sub>2</sub>, the electron and the hole are mainly present in adjacent weakly van der Waals coupled S-Mo-S monolayer planes along the  $c$ -axis [2]. Thus such exciton states are absent in monolayer films but appear in bilayer or thicker films [4]. It is also absent in the 3R form of TMDC crystal stacking [5]. In fact in bulk  $2H$ -MoS<sub>2</sub> this transition was originally thought to originate from the first excited state ( $2s$ ) [6] of the  $A$  exciton and then again wrongly identified as a transition at the  $H$  point of the Brillouin zone [7]. Unlike the ground state  $A_{1s}$  exciton, interlayer excitons have very large dipole moments leading to large Stark shifts with applied electric fields [3,8–10]. Consequently their transition energies can be tuned with moderate electric fields opening up the possibility of practical excitonic

devices. The strong coupling between interlayer excitons and phonons also leads to novel phenomenon like phonon Stark effect [11]. Interlayer excitons also give rise to very large second harmonic signal generation [12].

An important distinguishing feature of interlayer excitons in TMDCs is their large and positive Landé  $g$ -factor (LGF) value, very unlike the ground state  $A_{1s}$  and  $B_{1s}$  exciton LGF values, as shown in Table I for MoS<sub>2</sub>. Degenerate electron and hole energy levels in TMDCs undergo Zeeman splitting in a magnetic field. The spin, orbital and valley angular momentum composition of these levels and how they add up, determines the final Zeeman splitting energy and thereby the LGF value. In TMDCs this addition depends on novel phenomena such as spin-valley coupling [13,14] and spin-layer locking [15]. Measuring magneto-optical properties [16,17] of excitons has therefore been important for understanding the electronic structure of TMDCs and more recently their heterostructures where giant LGF values have been reported for interlayer excitons [18], Moiré trions [19] and trion-polaritons [20].

The exciton LGF is experimentally obtained by measuring the Zeeman splitting related energy shift ( $\Delta E_o$ ) of the exciton transition due to an external magnetic field ( $B$ ). By definition  $\Delta E_o = g_{ex} \mu_B B$  where  $\mu_B$  is the Bohr magneton and  $g_{ex}$  the exciton LGF. It has been reported that obtaining the LGF of some excitons in TMDCs is difficult with conventional magneto-luminescence/reflectance spectroscopy [21], even with very high fields of the order of tens of tesla. This is because of their large spectral broadening compared to  $\Delta E_o$  and typically moderate oscillator strength. We have used the magneto-optical Kerr effect (MOKE) spectroscopy to study excitons in bulk  $2H$ -MoS<sub>2</sub> and measure their LGF. In MOKE one directly measures the difference in the reflectance signal between right and left circularly polarized (RCP/LCP)

\*Contact author: thorsten.deilmann@uni-muenster.de

†Contact author: sangho10@tifr.res.in

TABLE I. Reported Landé  $g$ -factor of excitons in few-layer (ML: monolayer, BL: bilayer) and bulk  $2H$ -MoS<sub>2</sub>.

$g_{A_{1s}}$	$g_{B_{1s}}$	$g_{IL_A}$	$g_{IL_B}$	Measurement technique/sample
$-4.0 \pm 0.2$	$-4.65 \pm 0.17$			Circularly polarized reflectance contrast/ML [33]
$-4.6 \pm 0.1$	$-4.3 \pm 0.1$			Magneto transmission/ML [34]
$-3.38 \pm 0.05$	$-4.06 \pm 0.07$			Magnetic circular dichroism/ML [35]
$\sim -4.0$		$\sim 8.0$		Circularly polarized reflectance contrast/BL [21]
$-4.0 \pm 0.3$		$6.6 \pm 0.3, 7.2 \pm 0.3^b$		Faraday rotation in transmission/BL [36]
$-3.1 \pm 0.1$	$-2.5 \pm 0.3$	$12 \pm 1^a$		Magnetic circular dichroism/bulk [37]
$-2.5 \pm 0.5$		$9.7 \pm 2.5$		Magneto-modulated reflectance/bulk [38]
$-3.1 \pm 0.2$	$-3.0 \pm 0.4$	$10.9 \pm 0.8$	$10.6 \pm 1.5$	Magneto-optical Kerr effect/bulk [this study]

<sup>a</sup> $IL_A$  wrongly identified as  $A_{2s}$ .

<sup>b</sup> $IL_A$  is split.

light. The MOKE signal amplitude is proportional to  $\Delta E_o$  and enables measurement of  $\Delta E_o$  as small as  $\sim 100$   $\mu$ eV with moderate  $B$ , even when spectral features have tens of meV broadening [22]. We show that the MOKE spectrum of  $2H$ -MoS<sub>2</sub> at higher energies reveals the existence of a new exciton transition and thereafter verify its presence using photoreflectance (PR) spectroscopy. We try to establish the origins of this exciton through an understanding of its LGF value based on an approximate phenomenological model. We also performed *ab initio* calculations based on the density functional theory (DFT) and many-body perturbation theory [GW + Bethe-Salpeter equation (BSE)] to investigate exciton resonances over an extended energy range.

## II. EXPERIMENTAL DETAILS

The samples used in this study were bulk flakes exfoliated from natural  $2H$ -MoS<sub>2</sub> crystals and supported on polished sapphire substrates. We performed MOKE spectroscopy in polar geometry using a mirror arrangement [23], with a photoelastic modulator (PEM) for polarization modulation [24]. For doing measurements on clean flat regions of the flakes, a microscope like optical arrangement was included that enabled spatial resolution down to 25  $\mu$ m [25]. Two of the mirrors had a twisted periscope arrangement for transporting light with minimal change in its circular polarization state. A Jones matrix analysis of the setup was done to account for the effect of different optical elements, including beam splitters, on the polarization state of the probe light and appropriate corrections were made. The probe beam was obtained by dispersing light from a 75 W Xe lamp using a 0.15 m focal length monochromator. The detector was a photomultiplier tube and two lock-in amplifiers (LIA) were used for phase sensitive detection of the signals at the first and second harmonic of the PEM modulation frequency. Magnetic fields up to 2.0 T were obtained with a water cooled H-frame electromagnet. The samples were cooled using a liquid-nitrogen cryostat with optical access. For PR measurements, the pump beam was a 532-nm laser mechanically chopped at 175 Hz, and the signal proportional to change in intensity of the reflected probe light was measured using a LIA. This setup also had high spatial resolution capability. The authenticity of the measured MOKE spectrum was verified by checking its phase reversal due to reversing the direction of the magnetic field and also using

a Kramers-Kronig analysis. See Supplemental Material [26] and Refs. [27–30] therein.

## III. RESULTS AND DISCUSSION

Figure 1 shows the measured reflectance spectrum of  $2H$ -MoS<sub>2</sub> at 78 K, where three prominent exciton transitions are identified, the ground state  $A_{1s}$ ,  $B_{1s}$  excitons and the  $IL_A$  exciton [3]. The features below 1.89 eV arise from thin film interference oscillations in the sub-band-gap region of  $2H$ -MoS<sub>2</sub>. As depicted in Fig. 2, the ground state  $A_{1s}$  exciton involves electrons in one of two narrowly split conduction bands (CB1, CB2) and holes in the top valence band (VB1), at the  $K$  points of the Brillouin zone. The ground state  $B_{1s}$  exciton involves holes in the next highest valence band (VB2). In both the  $A_{1s}$  and  $B_{1s}$  state, the electron and hole are mostly confined in the same S-Mo-S layer [2,3,31]. The third  $IL_A$  which lies  $\sim 43$  meV above  $A_{1s}$  in energy, is the interlayer exciton transition described previously [2,3]. The optical polarization selection rules are based on DFT-BSE results [2]. They are a consequence of the exciton wave function and the mirrored Brillouin zone in every second layer. In the  $IL_A$  state the electron mainly resides in a S-Mo-S layer adjacent to the layer containing the hole in VB1, as indicated in Fig. 2.

Figure 3 shows the MOKE ellipticity  $\eta$  and rotation  $\phi$  spectrum of  $2H$ -MoS<sub>2</sub> at energies around the  $A_{1s}$  transition, measured with a magnetic field  $B = 2$  T. This is after subtracting from each a background spectrum measured with  $B = 0$  T. Both spectra show two features that can be attributed to  $A_{1s}$  and  $IL_A$  excitons by comparing their energy positions

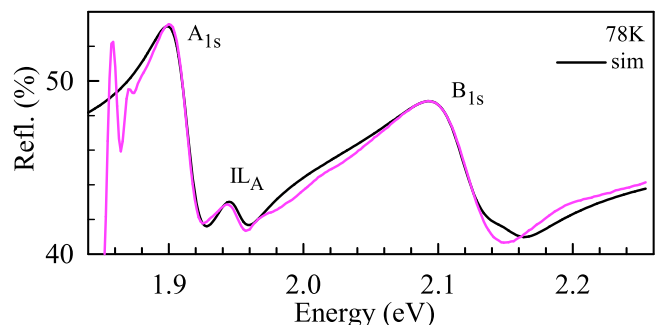


FIG. 1. Reflectance spectrum of bulk  $2H$ -MoS<sub>2</sub> showing previously identified dominant exciton transitions.

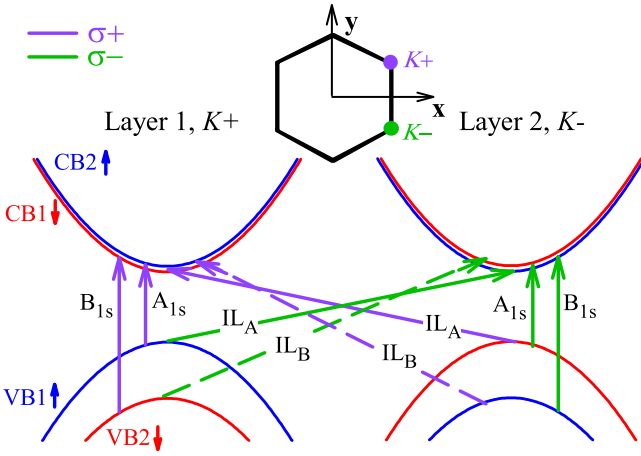


FIG. 2. Schematic showing the energy-crystal momentum dispersion for two adjacent S-Mo-S layers and circular polarization ( $\sigma+$ ,  $\sigma-$ ) dependent intralayer and interlayer exciton transitions in  $2H$ -MoS<sub>2</sub>. The first Brillouin zone of a single layer is shown on top, identifying the  $K+$  and  $K-$  points.

with the corresponding features in Fig. 1. As mentioned before the magnitude of the MOKE signal is proportional to the net shift in the exciton transition energy arising from Zeeman splitting of the electron and hole levels and it determines the magnitude of the LGF. The phase of the exciton MOKE signal is set by the direction of the exciton transition energy shift, whether to higher or lower energies, and therefore determines the sign of the LGF. Now note that in MOKE the  $IL_A$  feature in Fig. 3 has similar magnitude but opposite phase compared to the  $A_{1s}$  feature, although the oscillator strength of  $IL_A$  is much weaker than that of  $A_{1s}$  as seen from Fig. 1. This indicates that  $IL_A$  undergoes a larger shift in transition energy than  $A_{1s}$  and in the opposite direction, which implies that  $g_{IL_A}$  has larger magnitude opposite sign relative to  $g_{A_{1s}}$ . We estimated the LGF value from such data by comparing it with first-principles simulation [26], starting from the Lorentz

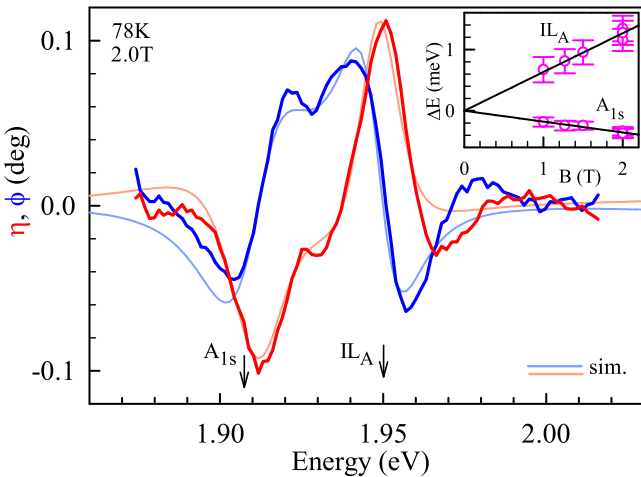


FIG. 3. MOKE Ellipticity  $\eta$  and rotation  $\phi$  spectrum of bulk  $2H$ -MoS<sub>2</sub> around the  $A_{1s}$  exciton transition for  $B = 2$  T. The simulations consider  $A_{1s}$  and  $IL_A$  exciton contributions. The inset shows variation of measured exciton Zeeman splitting with applied magnetic field.

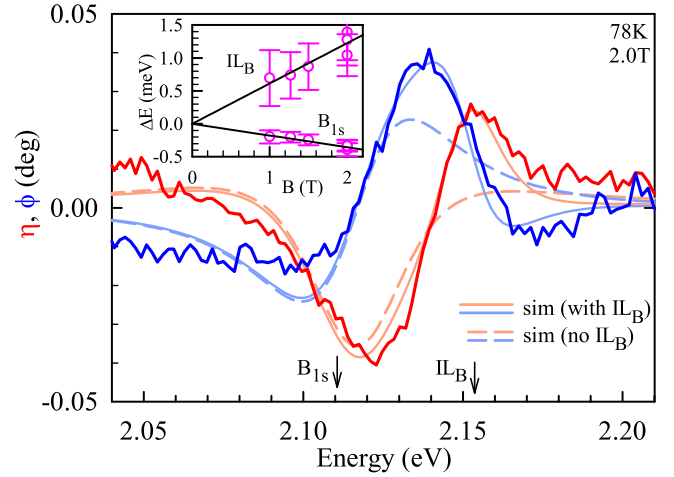


FIG. 4. MOKE Ellipticity  $\eta$  and Rotation  $\phi$  spectrum of bulk  $2H$ -MoS<sub>2</sub> around the  $B_{1s}$  exciton transition. One of the simulations considers both  $B_{1s}$  and  $IL_B$  exciton contributions (thin continuous line) and other only  $B_{1s}$  (dashed line). The inset shows variation of measured exciton Zeeman splitting with applied magnetic field.

oscillator model for the exciton's contribution to the dielectric function and then invoking Zeeman splitting of electron and hole levels. A second method that directly estimates  $\eta$  using the derivative of the measured reflectance spectrum [26,32] was also used for verification. These procedures are described in the Supplemental Material. The best fit simulated spectra are also shown in Fig. 3. The average LGF values for  $A_{1s}$  and  $IL_A$  from several measurements were  $g_{A_{1s}} = -3.1 \pm 0.2$ ,  $g_{IL_A} = 10.9 \pm 0.8$ . These values compare well with previous estimates that used other techniques as listed in Table I, especially for bulk  $2H$ -MoS<sub>2</sub>.

Figure 4 shows the MOKE ellipticity  $\eta$  and rotation  $\phi$  spectrum at 2 T at energies around the  $B_{1s}$  transition. Unlike the MOKE spectrum around  $A_{1s}$ , here we cannot immediately discern two spectral features. However if we try to simulate and fit this  $\eta$  and  $\phi$  spectrum by considering only a single  $B_{1s}$  exciton transition, the fit is significantly poor at the high energy side around 2.15 eV. Once we introduce an additional transition, which for now we label as  $IL_B$ , we get a good fit. Plots for fits with and without  $IL_B$  are shown in Fig. 4. The LGF values we obtained were  $g_{B_{1s}} = -3.0 \pm 0.4$ ,  $g_{IL_B} = 10.6 \pm 1.5$ . It is clear from Fig. 1 that  $B_{1s}$  has much larger broadening than  $A_{1s}$  and therefore this larger broadening is perhaps not allowing us to explicitly resolve the second weak feature  $IL_B$  in either reflectance or MOKE. To further verify that there is indeed another exciton transition there, we performed laser modulated PR spectroscopy. The PR spectrum around  $B_{1s}$  transition is shown in Fig. 5 where we clearly see two distinct transitions, one around the energy of  $B_{1s}$  and the other around 2.16 eV where  $IL_B$  was seen in the MOKE spectrum. In fact the  $IL_B$  feature is more prominent in PR, which we will discuss below. Fitting Aspnes' derivative functional form line shape function with redefined parameters [39] to this PR spectrum, we get the transition energies for  $B_{1s}$  and  $IL_B$  as 2.122 eV and 2.162 eV, respectively.

The large and positive sign of the LGF of  $IL_B$  transition is very similar to that of  $IL_A$  and the feature arises  $\sim 40$  meV on the higher energy side of  $B_{1s}$ , just like  $IL_A$  does relative

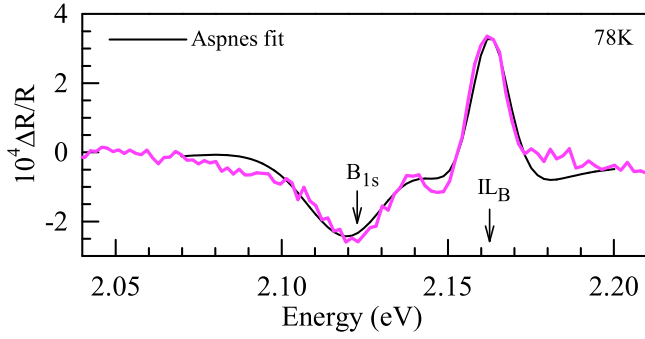


FIG. 5. Photoreflectance spectrum of  $2H$ - $\text{MoS}_2$  around the  $B_{1s}$  exciton transition energy showing clear evidence of an additional  $IL_B$  exciton transition.

to  $A_{1s}$ . This indicates that  $IL_B$  could be another interlayer type exciton similar to  $IL_A$ , but is mainly associated with the VB2 of the adjacent S-Mo-S layer as indicated in Fig. 2. More evidence supports this, the first one is related to the PR signal amplitude. An exciton related resonant feature in a reflectance (R) spectrum depends on the exciton oscillator strength  $A$ , broadening  $\Gamma$  and transition energy  $E_o$ . In PR, one measures the change in reflectance ( $\Delta R$ ), due to the sample being perturbed by a second pump laser beam. Therefore a normalized PR spectrum ( $\Delta R/R$ ) is like a derivative of the R spectrum, enabling it to pick up weak transitions over a large background R signal. The strength of the exciton PR signal depends directly on the extent of perturbation induced changes in the exciton parameters such as oscillator strength, broadening and transition energy. Furthermore, unlike  $A_{1s}$  or  $B_{1s}$  intralayer excitons where the electron and hole are confined to the same S-Mo-S layer, in the interlayer exciton state they are in adjacent S-Mo-S layers along the  $c$ -axis [2,3]. Due to the weak van der Waals coupling along the  $c$ -axis, states which are spread along the  $c$ -axis are much more sensitive to perturbation [3,40]. Thus although an interlayer exciton may have a weak oscillator strength and not show up in R, it is perturbed much more relative to that of an intralayer exciton, making it possible for the interlayer exciton to show up prominently in PR. This is indeed the case, as one can see in the PR spectrum of  $2H$ - $\text{MoS}_2$  around  $B_{1s}$  in Fig. 5 that the feature identified as  $IL_B$  is stronger than that for  $B_{1s}$ . In contrast, in the reflectance spectrum in Fig. 1 an  $IL_B$  feature is hardly discernible while  $B_{1s}$  is quite strong. We note that the possibility of an  $IL_B$  exciton in bilayer  $\text{MoS}_2$  had been theoretically predicted [4] earlier and in case of bilayer  $\text{MoSe}_2$  its LGF was predicted to have a large positive value [41].

#### A. Approximate model for Landé $g$ -factor

The second evidence for  $IL_B$  being an interlayer comes from the origin of  $g_{IL_B}$  sign and magnitude, which we estimate using an approximate additive model for exciton LGF as follows. We consider the  $B_{1s}$  exciton first which involves electrons and holes in the same S-Mo-S layer as indicated in Fig. 2. The electrons are in CB1 and holes in VB2 at the  $K$  points of the Brillouin zone. There are three angular momentum contributions to the LGF of carriers in TMDC materials, the spin, the orbital and the valley angular momentum. As

a simple first approximation the LGF contributions due to spin ( $g_s$ ), orbital ( $g_o$ ) and valley ( $g_v$ ) angular moments can be added, as was done in case of few-layer TMDCs [33,42]. At the  $K$  points, the orbital contribution at the top of the VBs comes mostly from  $d_{x^2-y^2} \pm id_{xy}$  [43] with quantum number  $m_j = \pm 2$  and the holes have  $g_o^h \sim \pm 2$  at two adjacent inequivalent  $K+$ ,  $K-$  valleys, respectively [33]. The CB bottom has mainly  $d_{z^2}$  orbital character [43] with  $m_j = 0$  and thus for electrons we get  $g_o^e \sim 0$  in both valleys [33]. The valley angular momentum gives a contribution  $g_v \sim \pm m_o/m^*$  at  $K+$ ,  $K-$  valleys, respectively, where  $m^*/m_o$  represents the effective mass ratio of the carriers [33,44]. The electron and hole effective masses for motion in the  $x-y$  plane determined by the energy-momentum dispersion around the  $K$  points in bulk  $2H$ - $\text{MoS}_2$  are similar [45] with  $m^*/m_o \sim 0.5$ , therefore  $g_v^{e,h} \sim \pm 2$  at  $K+$ ,  $K-$  respectively. The circular polarization selection rules for such exciton transitions have been calculated before [2] and are shown schematically in Fig. 2. Therefore for the  $B_{1s}$  exciton, we can express the shift in transition energy  $\Delta E_o$ , at the  $K+$  and  $K-$  valleys for RCP and LCP light, respectively, for an applied magnetic field  $B$  as

$$\Delta E_o^{\sigma+}(B_{1s}) = [g_s^{e,K+} + g_o^{e,K+} + g_v^{e,K+} - \{g_s^{h,K+} + g_o^{h,K+} + g_v^{h,K+}\}] \mu_B B \quad (1)$$

and

$$\Delta E_o^{\sigma-}(B_{1s}) = [g_s^{e,K-} + g_o^{e,K-} + g_v^{e,K-} - \{g_s^{h,K-} + g_o^{h,K-} + g_v^{h,K-}\}] \mu_B B. \quad (2)$$

The electron/hole spin orientations are locked [14] in  $K+$  and  $K-$  valleys of such TMDC semiconductors as shown in Fig. 2 and these orientations are preserved in an optical transition. Also the carriers are in the same valley, so both the spin and valley contributions in the above equations cancel out, leaving us with only the orbital contributions  $-g_o^{h,K+} = -2$  for RCP and  $-g_o^{h,K-} = 2$  for LCP polarization. The difference in the  $B_{1s}$  exciton transition energy between RCP and LCP light is then  $\Delta E_o^{\sigma+} - \Delta E_o^{\sigma-} = -4\mu_B B$ , which gives the exciton LGF as  $g_{B_{1s}} = -4$ . This value is strictly true for a single S-Mo-S layer in the absence of interlayer interactions. Our measured  $g_{B_{1s}}$  value is similar both in terms of sign and magnitude. As such in bulk materials the LGF value can be lower [46,47] so it is consistent with other values mentioned in Table I.

Next we consider what is expected for an interlayer type  $IL_B$  exciton where two adjacent S-Mo-S layers are involved. In  $2H$ - $\text{MoS}_2$  there is a  $180^\circ$  in-plane twist between adjacent S-Mo-S layers along the  $c$ -axis, also the spin locking orientation between adjacent layers is reversed [15,48]. Therefore in  $k$  space to conserve crystal momentum one will have to consider transitions between  $K_1+$  point of layer 1 to  $K_2-$  of layer 2 as indicated by the long tilted arrows in Fig. 2. Also the exciton will involve a hole in VB2 of one layer and electron in CB2 of the adjacent layer. In this case, the LCP light will excite such an interlayer exciton, comprising of a hole at  $K_1+$  and electron at  $K_2-$ . The shift in the transition energy  $\Delta E_o$  of  $IL_B$  exciton for LCP light, for an applied magnetic field  $B$  will be

$$\Delta E_o^{\sigma-}(IL_B) = [g_s^{e,K_2-} + g_o^{e,K_2-} + g_v^{e,K_2-} - \{g_s^{h,K_1+} + g_o^{h,K_1+} + g_v^{h,K_1+}\}] \mu_B B. \quad (3)$$

Similarly with RCP light one can excite an  $IL_B$  exciton comprising of a hole in the  $K_2-$  valley and an electron in the  $K_1+$  valley and the shift in the transition energy  $\Delta E_o$ , for an applied magnetic field  $B$  will be

$$\Delta E_o^{\sigma+}(IL_B) = [g_s^{e,K_1+} + g_o^{e,K_1+} + g_v^{e,K_1+} - \{g_s^{h,K_2-} + g_o^{h,K_2-} + g_v^{h,K_2-}\}] \mu_B B. \quad (4)$$

Since electron/hole spin orientations are preserved in these transitions, the net spin angular momentum contribution to LGF will again be zero. Only the orbital and valley angular momentum will contribute. Using numbers mentioned earlier, the difference in the  $IL_B$  exciton transition energy between RCP and LCP light becomes  $\Delta E_o^{\sigma+} - \Delta E_o^{\sigma-} = +12\mu_B B$ , yielding an exciton LGF value  $g_{IL_B} = +12$ . This shows that for an interlayer exciton we expect a large positive value of LGF and it is consistent with our measure  $g_{IL_B}$ . The  $IL_B$  ( $IL_A$ ) exciton transition is at a higher energy than  $B_{1s}$  ( $A_{1s}$ ) most likely because it has a lower binding energy due to the electron and hole being more separated since they are in adjacent S-Mo-S layers, unlike  $B_{1s}$  ( $A_{1s}$ ) where they are in the same S-Mo-S layer [3]. We note that the high energy feature seen in PR around 2.16 eV was earlier wrongly interpreted [7] as a new exciton transition at the  $H$  point of the Brillouin zone. It was later shown that due to a saddle point like energy-crystal momentum curvature at the  $H$  point, an exciton cannot be sustained there [3]. With the present estimate of LGF for this transition, we can now correctly identify it as an  $IL_B$  exciton.

### B. First-principles results

In this section we discuss the results of our calculations based on first principles. We use the experimental lattice structure of the  $2H$  phase [49] and employ a hierarchy of methods. For the optimization of the internal structure until all forces are below  $10^{-4}$  Ry/ $a_B$ , we use a  $21 \times 21 \times 3$  k mesh, the local density approximation, a basis of localized Gaussian orbitals ( $s$ ,  $p$ ,  $d$ , and  $s^*$ , in total 30 per atom), and norm-conserving pseudopotentials which include the spin-orbit coupling [50,51]. To improve the description of the electronic properties, many-body perturbation theory calculations, i.e.,  $GW$  in the  $GdW$  approximation [52], are performed with a plane wave cutoff of 2.5 Ry and k grid of  $21 \times 21 \times 4$  points. The optical properties were calculated by solving the BSE [53] employing a grid of  $36 \times 36 \times 6$  points.

Figure 6 shows the calculated optical absorption spectrum of bulk  $2H$ -MoS<sub>2</sub>. Below the direct band gap of  $E_g = 2.18$  eV we find two clear peaks which correspond to the  $A_{1s}$  and  $IL_A$  excitons. Higher excited states are present close to the band gap, however, with the employed broadening of 15 meV they are hardly visible in the spectrum. The  $A_{1s}$  and  $IL_A$  character is identified through the corresponding exciton wave function as discussed in previous studies [2]. Above  $E_g$ , a continuum of states is present and it is nearly impossible to converge them even after employing huge k-grids. On top of this continuum, additional resonances from the  $B$  excitons are seen in Fig. 6. The dominant resonance here can be identified as  $B_{1s}$ , and the weaker resonance on its high energy side, is exactly where we observe  $IL_B$  in experiments. Also the calculated energy difference between  $B_{1s}$  and  $IL_B$  is  $\sim 40$  meV, similar to that

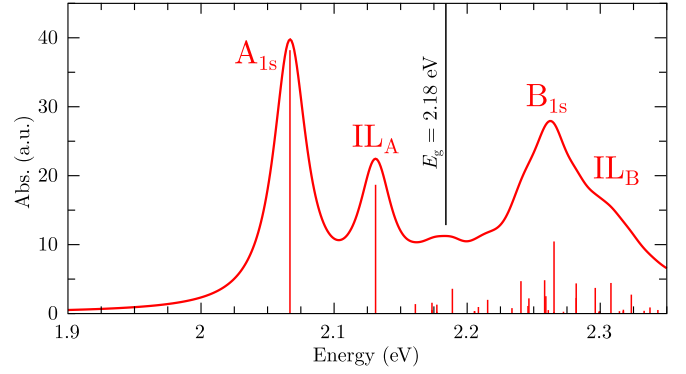


FIG. 6. Calculated absorption spectrum of bulk  $2H$ -MoS<sub>2</sub>. A Lorentzian with a broadening of 15 meV was used for all peaks in the spectrum.

between  $A_{1s}$  and  $IL_A$  which is  $\sim 60$  meV. Due to coupling with the continuum, the  $B$  exciton resonance is built up from many transitions (vertical red lines below the corresponding peaks), in contrast to the  $A$  series excitons which typically have one strong transition. This leads to the overall broadening of the exciton states around  $B_{1s}$  and weakened resonance, which is also indicated in the experimental data in Fig. 1. Thus although we have evidence for an  $IL_B$  exciton, because of the presence of several transitions around these resonances, a unique identification of the state by getting the exciton wavefunction, is not possible. Finally, it had been suggested earlier [54] that the  $IL_A$  exciton state can be considered as a mixture of an optically dark charge transfer exciton involving VB1 with an intralayer  $B_{1s}$  exciton, which provides the oscillator strength. In our case the equivalent would be a dark charge transfer exciton involving VB2 which gains strength from mixing with an intralayer  $A_{1s}$  exciton.

### IV. CONCLUSION

In conclusion, we first showed that using MOKE spectroscopy with moderate fields up to 2 T, one is able to measure the Landé  $g$ -factor of known exciton transitions in  $2H$ -MoS<sub>2</sub> which agrees well with values reported in the literature. Thereafter we showed evidence for a new  $IL_B$  exciton transition in the MOKE spectrum and verified its existence independently through PR spectroscopy. This new interlayer type exciton is suggested to be associated with the second highest valance band at the  $K$  point of the Brillouin zone of  $2H$ -MoS<sub>2</sub>. Using an approximate model to account for the Landé  $g$ -factor contribution from spin, orbital, and valley angular momentum, we showed that  $g_{IL_B}$  should have a high positive value which is consistent with what we measured and in contrast to the lower  $g_{B_{1s}}$  value and its negative sign. Finally, results from DFT-BSE calculations also show an exciton state on the higher energy side of  $B_{1s}$ , where we observe  $IL_B$  in experiments.

### ACKNOWLEDGMENTS

The authors thank A. Arora and V. Jindal for many useful discussions, and V. Sugunakar for help with instrumentation. S.G. acknowledges funding from the Department of Atomic Energy, Government of India through Project No. RTI 4003.

T.D. acknowledges financial support from the Deutsche Forschungsgemeinschaft (DFG, German Research Foundation) through Project No. 426726249 (DE 2749/2-1 and DE 2749/2-2). The authors acknowledge the Gauss Centre for Su-

percomputing e.V. [55] for funding this project by providing computing time through the John von Neumann Institute for Computing (NIC) on the GCS Supercomputer JUWELS [56] at Jülich Supercomputing Centre (JSC).

- 
- [1] G. Wang, A. Chernikov, M. M. Glazov, T. F. Heinz, X. Marie, T. Amand, and B. Urbaszek, *Colloquium: Excitons in atomically thin transition metal dichalcogenides*, *Rev. Mod. Phys.* **90**, 021001 (2018).
- [2] A. Arora, M. Druppel, R. Schmidt, T. Deilmann, R. Schneider, M. R. Molas, P. Marauhn, S. M. de Vasconcellos, M. Potemski, M. Rohlfing, and R. Bratschitsch, Interlayer excitons in a bulk van der Waals semiconductor, *Nat. Commun.* **8**, 639 (2017).
- [3] V. Jindal, D. Jana, T. Deilmann, and S. Ghosh, Interlayer and excited-state exciton transitions in bulk 2H-MoS<sub>2</sub>, *Phys. Rev. B* **102**, 235204 (2020).
- [4] I. C. Gerber, E. Courtade, S. Shree, C. Robert, T. Taniguchi, K. Watanabe, A. Balocchi, P. Renucci, D. Lagarde, X. Marie, and B. Urbaszek, Interlayer excitons in bilayer MoS<sub>2</sub> with strong oscillator strength up to room temperature, *Phys. Rev. B* **99**, 035443 (2019).
- [5] I. Paradisanos, S. Shree, A. George, N. Leisgang, C. Robert, K. Watanabe, T. Taniguchi, R. J. Warburton, A. Turchanin, X. Marie, I. C. Gerber, and B. Urbaszek, Controlling interlayer excitons in MoS<sub>2</sub> layers grown by chemical vapor deposition, *Nat. Commun.* **11**, 2391 (2020).
- [6] E. Fortin and F. Raga, Excitons in molybdenum disulphide, *Phys. Rev. B* **11**, 905 (1975).
- [7] N. Saigal and S. Ghosh, H-point exciton transitions in bulk MoS<sub>2</sub>, *Appl. Phys. Lett.* **106**, 182103 (2015).
- [8] N. Leisgang, S. Shree, I. Paradisanos, L. Sponfeldner, C. Robert, D. Lagarde, A. Balocchi, K. Watanabe, T. Taniguchi, X. Marie, R. J. Warburton, I. C. Gerber, and B. Urbaszek, Giant Stark splitting of an exciton in bilayer MoS<sub>2</sub>, *Nat. Nanotechnol.* **15**, 901 (2020).
- [9] E. Lorchat, M. Selig, F. Katsch, K. Yumigeta, S. Tongay, A. Knorr, C. Schneider, and S. Höfling, Excitons in bilayer MoS<sub>2</sub> displaying a colossal electric field splitting and tunable magnetic response, *Phys. Rev. Lett.* **126**, 037401 (2021).
- [10] Y. Zhao, L. Du, S. Yang, J. Tian, X. Li, C. Shen, J. Tang, Y. Chu, K. Watanabe, T. Taniguchi, R. Yang, D. Shi, Z. Sun, Y. Ye, W. Yang, and G. Zhang, Interlayer exciton complexes in bilayer MoS<sub>2</sub>, *Phys. Rev. B* **105**, L041411 (2022).
- [11] Z. Huang, Y. Bai, Y. Zhao, L. Liu, X. Zhao, J. Wu, K. Watanabe, T. Taniguchi, W. Yang, D. Shi, Y. Xu, T. Zhang, Q. Zhang, P. H. Tan, Z. Sun, S. Meng, Y. Wang, L. Du, and G. Zhang, Observation of phonon Stark effect, *Nat. Commun.* **15**, 4586 (2024).
- [12] S. Shree, D. Lagarde, L. Lombez, C. Robert, A. Balocchi, K. Watanabe, T. Taniguchi, X. Marie, I. C. Gerber, M. M. Glazov, L. E. Golub, B. Urbaszek, and I. Paradisanos, Interlayer exciton mediated second harmonic generation in bilayer MoS<sub>2</sub>, *Nat. Commun.* **12**, 6894 (2021).
- [13] D. Xiao, G. B. Liu, W. Feng, X. Xu, and W. Yao, Coupled spin and valley physics in monolayers of MoS<sub>2</sub> and other group-VI dichalcogenides, *Phys. Rev. Lett.* **108**, 196802 (2012).
- [14] K. F. Mak, K. He, J. Shan, and T. F. Heinz, Control of valley polarization in monolayer MoS<sub>2</sub> by optical helicity, *Nat. Nanotechnol.* **7**, 494 (2012).
- [15] A. M. Jones, H. Yu, J. S. Ross, P. Klement, N. J. Ghimire, J. Yan, D. G. Mandrus, W. Yao, and X. Xu, Spin-layer locking effects in optical orientation of exciton spin in bilayer WSe<sub>2</sub>, *Nat. Phys.* **10**, 130 (2014).
- [16] X. Xu, W. Yao, D. Xiao, and T. F. Heinz, Spin-layer locking effects in optical orientation of exciton spin in bilayer WSe<sub>2</sub>, *Nat. Phys.* **10**, 343 (2014).
- [17] A. Arora, Magneto-optics of layered two-dimensional semiconductors and heterostructures: Progress and prospects, *J. Appl. Phys.* **129**, 120902 (2021).
- [18] P. Nagler, M. V. Ballottin, A. A. Mitioglu, F. Mooshammer, N. Paradiso, C. Strunk, R. Huber, A. Chernikov, P. C. M. Christianen, C. Schüller, and T. Korn, Giant magnetic splitting inducing near-unity valley polarization in van der Waals heterostructures, *Nat. Commun.* **8**, 1551 (2017).
- [19] X. Wang, J. Zhu, K. L. Seyler, P. Rivera, H. Zheng, Y. Wang, M. He, T. Taniguchi, K. Watanabe, J. Yan, D. G. Mandrus, D. R. Gamelin, W. Yao, and X. Xu, Moiré trions in MoSe<sub>2</sub>/WSe<sub>2</sub> heterobilayers, *Nat. Nanotechnol.* **16**, 1208 (2021).
- [20] T. P. Lyons, D. J. Gillard, C. Leblanc, J. Puebla, D. D. Solnyshkov, L. Klompmaker, I. A. Akimov, C. Louca, P. Muduli, A. Genco, M. Bayer, Y. Otani, G. Malpuech, and A. I. Tartakovskii, Giant effective Zeeman splitting in a monolayer semiconductor realized by spin-selective strong light-matter coupling, *Nat. Photon.* **16**, 632 (2022).
- [21] A. O. Slobodeniuk, Ł. Bala, M. Koperski, M. R. Molas, P. Kossacki, K. Nogajewski, M. Bartos, K. Watanabe, T. Taniguchi, C. Faugeras, and M. Potemski, Fine structure of K excitons in multilayers of transition metal dichalcogenides, *2D Mater.* **6**, 025026 (2019).
- [22] A. Arora, A. Mandal, S. Chakrabarti, and S. Ghosh, Magneto-optical Kerr effect spectroscopy based study of Landé g-factor for holes in GaAs/AlGaAs single quantum wells under low magnetic fields, *J. Appl. Phys.* **113**, 213505 (2013).
- [23] A. Arora, S. Ghosh, and V. Sugunakar, A mirror based polar magneto-optical Kerr effect spectroscopy arrangement, *Rev. Sci. Instrum.* **82**, 123903 (2011).
- [24] K. Sato, Measurement of magneto-optical Kerr effect using piezo-birefringent modulator, *Jpn. J. Appl. Phys.* **20**, 2403 (1981).
- [25] D. Das and S. Ghosh, Polar magneto-optical Kerr effect spectroscopy with a microscope arrangement for studies on 2D materials, *Rev. Sci. Instrum.* **95**, 083904 (2024).
- [26] See Supplemental Material at <http://link.aps.org/supplemental/10.1103/PhysRevB.110.115201> for (i) how the Landé g-factor is estimated from comparing first principles simulations with measured MOKE spectrum and also directly from the measured R spectrum and (ii) checking the authenticity of the measured

- MOKE spectrum using magnetic field reversal and Kramers-Kronig analysis.
- [27] R. M. A. Azzam and N. M. Bashara, *Ellipsometry and Polarized Light* (North-Holland, New York, 1977).
- [28] E. Hecht, *Optics*, 3rd ed. (Addison-Wesley, Boston, 1998).
- [29] C. Klingshirn, *Semiconductor Optics* (Springer, Berlin, 2005).
- [30] P. Kielar, Magneto-optical polar Kerr effect and dispersion relations, *J. Opt. Soc. Am. B* **11**, 854 (1994).
- [31] A. Molina-Sanchez, D. Sangalli, K. Hummer, A. Marini, and L. Wirtz, Effect of spin-orbit interaction on the optical spectra of single-layer, double-layer, and bulk MoS<sub>2</sub>, *Phys. Rev. B* **88**, 045412 (2013).
- [32] Y. H. Chen, X. L. Ye, B. Xu, Z. G. Wang, and Z. Yang, Large g-factors of higher-lying excitons detected with reflectance difference spectroscopy in GaAs-based quantum wells, *Appl. Phys. Lett.* **89**, 051903 (2006).
- [33] A. V. Stier, K. M. McCreary, B. T. Jonker, J. Kono, and S. A. Crooker, Exciton diamagnetic shifts and valley Zeeman effects in monolayer WS<sub>2</sub> and MoS<sub>2</sub> to 65 Tesla, *Nat. Commun.* **7**, 10643 (2016).
- [34] A. A. Mitioglu, K. Galkowski, A. Surrente, L. Klopotoski, D. Dumcenco, A. Kis, D. K. Maude, and P. Plochocka, Magnetoexcitons in large area CVD-grown monolayer MoS<sub>2</sub> and MoSe<sub>2</sub> on sapphire, *Phys. Rev. B* **93**, 165412 (2016).
- [35] Y. J. Wu, C. Shen, Q. H. Tan, J. Shi, X. F. Liu, Z. H. Wu, J. Zhang, P. H. Tan, and H. Z. Zheng, Valley Zeeman splitting of monolayer MoS<sub>2</sub> probed by low-field magnetic circular dichroism spectroscopy at room temperature, *Appl. Phys. Lett.* **112**, 153105 (2018).
- [36] B. Carey, N. K. Wessling, P. Steeger, R. Schmidt, S. M. de Vasconcellos, R. Bratschitsch, and A. Arora, Giant Faraday rotation in atomically thin semiconductors, *Nat. Commun.* **15**, 3082 (2024).
- [37] M. Tanaka, H. Fukutani, and G. Kuwabara, Excitons in VI B transition metal dichalcogenides, *J. Phys. Soc. Jpn.* **45**, 1899 (1978).
- [38] D. Das, V. Jindal, V. Sugunakar, and S. Ghosh, Landé g Factor of excitons from circularly polarized low-field Magnetomodulated reflectance spectroscopy: Application to bulk 2H-MoS<sub>2</sub>, *Phys. Rev. Appl.* **19**, 064073 (2023).
- [39] S. Ghosh and H. T. Grahn, Photorefectance line shape of excitonic transitions analyzed with a redefined set of fitting parameters, *J. Appl. Phys.* **90**, 500 (2001).
- [40] V. Jindal, S. Bhuyan, T. Deilmann, and S. Ghosh, Anomalous behavior of the excited state of the A exciton in bulk WS<sub>2</sub>, *Phys. Rev. B* **97**, 045211 (2018).
- [41] Ł. Kipcza, A. O. Slobodeniuk, T. Woźniak, M. Bhatnagar, N. Zawadzka, K. Olkowska-Pucko, M. Grzeszczyk, K. Watanabe, T. Taniguchi, A. Babiński, and M. R. Molas, Analogy and dissimilarity of excitons in monolayer and bilayer of MoSe<sub>2</sub>, *2D Mater.* **10**, 025014 (2023).
- [42] M. Koperski, M. R. Molas, A. Arora, K. Nogajewski, M. Bartos, J. Wyzula, D. Vaclavkova, P. Kossacki, and M. Potemski, Orbital, spin and valley contributions to Zeeman splitting of excitonic resonances in MoSe<sub>2</sub>, WSe<sub>2</sub> and WS<sub>2</sub> monolayers, *2D Mater.* **6**, 015001 (2019).
- [43] G. B. Liu, W. Y. Shan, Y. Yao, W. Yao, and D. Xiao, Three-band tight-binding model for monolayers of group-VIB transition metal dichalcogenides, *Phys. Rev. B* **88**, 085433 (2013).
- [44] D. Xiao, W. Yao, and Q. Niu, Valley-contrasting physics in graphene: Magnetic moment and topological transport, *Phys. Rev. Lett.* **99**, 236809 (2007).
- [45] H. Peelaers and C. G. Van de Walle, Effects of strain on band structure and effective masses in MoS<sub>2</sub>, *Phys. Rev. B* **86**, 241401(R) (2012).
- [46] A. Arora, M. Koperski, A. Slobodeniuk, K. Nogajewski, R. Schmidt, R. Schneider, M. R. Molas, S. M. de Vasconcellos, R. Bratschitsch, and M. Potemski, Zeeman spectroscopy of excitons and hybridization of electronic states in few-layer WSe<sub>2</sub>, MoSe<sub>2</sub> and MoTe<sub>2</sub>, *2D Mater.* **6**, 015010 (2019).
- [47] T. Wozniak, P. E. Faria Junior, G. Seifert, A. Chaves, and J. Kunstmann, Exciton g-factors of van der Waals heterostructures from first-principles calculations, *Phys. Rev. B* **101**, 235408 (2020).
- [48] Z. Gong, G. B. Liu, H. Yu, D. Xiao, X. Cui, X. Xu, and W. Yao, Magnetoelectric effects and valley-controlled spin quantum gates in transition metal dichalcogenide bilayers, *Nat. Commun.* **4**, 2053 (2013).
- [49] Th. Böker, R. Severin, A. Müller, C. Janowitz, R. Manzke, D. Voss, P. Krüger, A. Mazur, and J. Pollmann, Band structure of MoS<sub>2</sub>, MoSe<sub>2</sub>, and  $\alpha$ -MoTe<sub>2</sub>: Angle-resolved photoelectron spectroscopy and *ab initio* calculations, *Phys. Rev. B* **64**, 235305 (2001).
- [50] D. R. Hamann, Generalized norm-conserving pseudopotentials, *Phys. Rev. B* **40**, 2980 (1989).
- [51] L. A. Hemstreet, C. Y. Fong, and J. S. Nelson, First-principles calculations of spin-orbit splittings in solids using nonlocal separable pseudopotentials, *Phys. Rev. B* **47**, 4238 (1993).
- [52] M. Drüppel, T. Deilmann, J. Noky, P. Marauhn, P. Krüger, and M. Rohlfing, Electronic excitations in transition metal dichalcogenide monolayers from an LDA+*GdW* approach, *Phys. Rev. B* **98**, 155433 (2018).
- [53] M. Rohlfing and S. G. Louie, Electron-hole excitations and optical spectra from first principles, *Phys. Rev. B* **62**, 4927 (2000).
- [54] T. Deilmann and K. S. Thygesen, Interlayer excitons with large optical amplitudes in layered van der Waals materials, *Nano Lett.* **18**, 2984 (2018).
- [55] [www.gauss-centre.eu](http://www.gauss-centre.eu).
- [56] D. Alvarez, JUWELS cluster and booster: Exascale pathfinder with modular supercomputing architecture at Juelich supercomputing centre, *JLSRF* **7**, A183 (2021).